CHEMISTRY

Carbon capture in polymer-based electrolytes

Yang Wang[1]†, Tony G. Feric[2,3]†, Jing Tang[1,4,5]†, Chao Fang[1,6], Sara T. Hamilton[3,7], David M. Halat[1,6], Bing Wu[1], Hasan Celik[8], Guanhe Rim[3,7], Tara DuBridge[1], Julianne Oshiro[1], Rui Wang[1,6], Ah-Hyung Alissa Park[2,3,7]*, Jeffrey A. Reimer[1,7,6]*

Nanoparticle organic hybrid materials (NOHMs) have been proposed as excellent electrolytes for combined CO_2 capture and electrochemical conversion due to their conductive nature and chemical tunability. However, CO_2 capture behavior and transport properties of these electrolytes after CO_2 capture have not yet been studied. Here, we use a variety of nuclear magnetic resonance (NMR) techniques to explore the carbon speciation and transport properties of branched polyethylenimine (PEI) and PEI-grafted silica nanoparticles (denoted as NOHM-I-PEI) after CO_2 capture. Quantitative ^{13}C NMR spectra collected at variable temperatures reveal that absorbed CO_2 exists as carbamates ($RHNCOO^-$ or $RR'NCOO^-$) and carbonate/bicarbonate (CO_3^{2-}/HCO_3^-). The transport properties of PEI and NOHM-I-PEI studied using ^1H pulsed-field-gradient NMR, combined with molecular dynamics simulations, demonstrate that coulombic interactions between negatively and positively charged chains dominate in PEI, while the self-diffusion in NOHM-I-PEI is dominated by silica nanoparticles. These results provide strategies for selecting adsorbed forms of carbon for electrochemical reduction.

INTRODUCTION

Over the past several decades, the rapid development of industries supporting intensive human activities has caused a rapid increase of CO_2 in the atmosphere, leading to pressing global warming via radiative forcing. To mitigate the effects of climate change, substantial efforts have been devoted to decarbonizing the industrial, chemical, and power sectors. Post-combustion carbon capture technologies, such as absorption in monoethanolamine solutions, have been developed over the last couple of decades and are considered the most industrially mature systems (*1*, *2*). However, the regeneration of CO_2 from aqueous amine solutions is energy intensive due to the large heat capacity of water, requiring up to 30% of the power output when applied as capture techniques in a coal-fired power plant (*3*). In addition, the transport of CO_2 for sequestration also increases the societal cost of carbon emission mitigation. Today, there are few large-scale CO_2 sequestration projects because, until the launch of recent tax incentive structure amendments, it was not economically feasible to capture and store CO_2 underground. As a result, there has been considerable interest in converting captured CO_2 to a variety of value-added products with a lower carbon intensity to provide a clear economic incentive that encourages the adoption of carbon management technologies more broadly. More recently, reactive capture and conversion have been proposed as an approach whereby CO_2 is captured and then converted in a single-reactor system, to avoid the energy penalty of regenerating the CO_2 capture medium and subsequently pressurizing and transporting the CO_2 before conversion (*4*). To realize these proposed energy reductions, efficient reactors and ingenious chemistries that couple CO_2 capture and conversion are urgently needed.

Combined carbon capture and reaction are ideally matched to renewable energy technologies in spite of intermittency and storage issues (*5*–*7*). The electrochemical conversion of CO_2 coupled with renewable energy is a promising option to mitigate the effects of greenhouse gas emissions while simultaneously producing value-added chemicals and fuels (*8*, *9*). Now, the CO_2 reduction reaction (CO_2RR) is limited by slow kinetics (*10*) as well as a typically low CO_2 solubility in aqueous electrolytes (e.g., 34 mM) (*9*, *11*). Despite remarkable breakthroughs in catalyst synthesis (*12*–*14*) and electrochemical reactor design (*12*, *15*, *16*), there is a paucity of understanding about the role of electrolytes in improving these electrochemical conversion pathways (*11*, *17*). Interactions between the electrolyte and electrode at the interface have been shown to noticeably stabilize their electrochemical reaction intermediates, thus highlighting the importance of the electrolyte phase in CO_2 reduction (*18*, *19*).

To overcome the limitation of mass transfer of CO_2 to the catalyst surface, nonaqueous electrolytes, such as acetonitrile and propylene carbonate, have been used (*9*, *11*). Moreover, additives to aqueous electrolytes such as ionic liquids (*18*, *20*), ligands (*21*), surfactants (*14*), deep eutectic solvents (*22*), and/or amines (*23*–*25*) have been found to act as cocatalysts for the CO_2RR owing to their remarkable ability to reduce the required overpotential, tune product selectivity, and improve reaction rates. The use of ionic liquids in the electrochemical conversion of CO_2 has been extensively studied, although the exact mechanism is still unclear due to the lack of operando electrochemical measurements (*9*, *26*). The experimental and computational evidence collected to date suggests that physical and chemical interactions between the ionic liquid and the reaction intermediates play a crucial role in facilitating the CO_2RR (*20*, *21*). Thus, it would be ideal to design an electrolyte with high CO_2 solubility and favorable interactions at the electrode-electrolyte interface that could enhance conversion rates while eliminating the energy-intensive solvent regeneration step associated with CO_2 absorption technologies.

[1]Department of Chemical and Biomolecular Engineering, College of Chemistry, UC Berkeley, Berkeley, CA 94720, USA. [2]Department of Chemical Engineering, Columbia University, New York, NY 10027, USA. [3]Lenfest Center for Sustainable Energy, Columbia University, New York, NY 10027, USA. [4]Department of Materials Science and Engineering, Stanford University, Stanford, CA 94305, USA. [5]Stanford Institute for Materials and Energy Sciences, SLAC National Accelerator Laboratory, 2575 Sand Hill Road, Menlo Park, CA 94025, USA. [6]Materials Sciences Division, Lawrence Berkeley National Laboratory, Berkeley, CA 94720, USA. [7]Department of Earth and Environmental Engineering, Columbia University, New York, NY 10027, USA. [8]College of Chemistry Nuclear Magnetic Resonance Facility (CoC-NMR), University of California, Berkeley, CA 94720, USA.
*Corresponding author. Email: ap2622@columbia.edu (A.-H.A.P.); reimer@berkeley.edu (J.A.R.)
†These authors contributed equally to this work.

Owing to their high CO_2 solubility (*27*), chemical tunability (*28*), and thermal-oxidative stability (*29*), liquid-like nanoparticle organic hybrid materials (NOHMs) are proposed as electrolyte additives for combined CO_2 capture and conversion applications (*30*). NOHMs are composed of organic polymers ionically or covalently tethered to an inorganic nanoparticle core, usually via a chemical linker (*31*, *32*). These materials have been extensively studied as water-lean CO_2 capture solvents (*33*, *34*) and electrode-stabilizing electrolyte additives for Li-metal batteries (*35*, *36*). Although NOHMs have been shown to appear as very promising candidates for energy storage applications, the main challenge associated with their use in electrochemical systems is their high viscosities in the neat state (*28*); thus, the addition of NOHMs to aqueous electrolytes has been recommended to overcome this limitation (*37*).

Because of their high ionic conductivity, CO_2-loaded aqueous amine solutions under certain reaction conditions have recently been demonstrated as media capable of hosting the efficient upgrade of CO_2 to compounds such as carbon monoxide or formate (*23*, *25*, *32*). We recently reported on the importance of the binding energy between polymer canopy functional groups and CO_2 toward the electrochemical conversion of CO_2 (*32*). For example, CO_2 captured by NOHM-I-PEI in the form of a carbamate was not able to be electrochemically converted at room temperature, while NOHMs containing ether groups along the polymer canopy were able to selectively form CO, the desired product for CO_2RR over silver nanoparticle catalysts, at very negative applied potentials (−1.2 V versus reversible hydrogen electrode) (*32*). Increasing the temperature of CO_2-loaded amine electrolytes was shown to lead to efficient CO_2 reduction, yet the role of the carbamate species in CO_2 conversion has recently been debated (*24*, *25*).

Here, we have prepared NOHM-I-PEI by ionically tethering branched PEI to ~10-nm silica nanoparticles, which works as an excellent CO_2 capture material (Fig. 1A) (*29*, *32*). After mixing the NOHM-I-PEI (Fig. 1B) with water and salt (e.g., $KHCO_3$) to form NOHM-based electrolytes, we measured the CO_2 capture capacity and transport properties (e.g., ionic conductivity and viscosity) as a function of NOHM-I-PEI concentration to understand how CO_2 loading affects properties that are relevant to electrochemical processes, such as the speciation of carbon species. In addition, we used a variety of nuclear magnetic resonance (NMR) techniques to further probe the reaction mechanisms, chemical equilibria, and transport behavior in these nanoscale-hybrid electrolyte systems. These results provide a detailed mechanism for CO_2 capture and, along with molecular dynamics simulations, show the role that these reactions play in the dynamics of the tethered PEI chains. Overall, the results of this study inform the optimal NOHM-I-PEI preparation and reaction conditions to enhance reactive capture and conversion of CO_2 in NOHM-based electrolytes.

RESULTS AND DISCUSSION

Effect of polymer tethering and salt on CO_2 capture capacity

The CO_2 capture capacity (P_{CO2} = 1 atm) of various PEI-based and NOHM-I-PEI–based fluids/electrolytes were measured by the CO_2 capture setup (fig. S1), and the results are summarized in Fig. 1 (C and D). There is an apparent linear relationship between the equilibrium CO_2 capture capacity and the concentration, measured in wt %, of PEI and NOHM-I-PEI (Fig. 1C), as expected. To provide proper quantification of the CO_2 capture in NOHM-I-PEI, water-ratio normalization [i.e., water content (λ_{H2O})] was applied, enabling the concentration of the PEI and NOHM-I-PEI samples to be directly comparable to one another (*37*). The water content (λ_{H2O}) can be determined by eqs. S1 and S2 shown in the Supplementary Materials (see table S1 for the conversion between water content and the polymer concentration). It can be found that this normalization results in a converging of these curves into a single curve (fig. S2), suggesting that polymer tethering does not markedly affect the amine efficiency of the polymer, which is especially useful given that ionically tethered NOHM-I-PEI systems have been shown to demonstrate substantially enhanced thermal stability over the untethered polymer (*27*). On the basis of the CO_2 capture capacity, the amine efficiency (α) of each sample can be calculated by eq. S3 shown in the Supplementary Materials. The amine efficiency of all samples was between 0.4 and 0.5 (fig. S3), which indicates that the resulting CO_2 capture process mainly consists of two reactions (Eqs. 8 and 9) with a molar ratio of 1:2 for CO_2 and amines, consistent with literature reports at similar experimental conditions (T = 25°C, P_{CO2} = 1 atm) (*38*–*40*).

The bulk CO_2 uptakes, as well as viscosity measurements, further suggest the efficacy of the NOHM-based electrolytes. Figure 1C shows that the addition of 0.1 M $KHCO_3$, one of the most common electrolytes used for CO_2 electrochemical reduction, negligibly affects their total CO_2 capture capacity in the concentration range of 10 to 30 wt % (Fig. 1D). The viscosity of PEI and NOMH-I-PEI solutions (Fig. 1D and fig. S4) increases rapidly in both solutions when the concentration increases over 20 wt % or λ decreases below 10 (fig. S4). We surmise that the CO_2 uptake rate in PEI and NOMH-I-PEI solutions will become mass-transfer limited as the concentration increases over ~20 wt % (or λ decreases below 10). This demonstrates that the optimal concentration of NOHM-I-PEI for CO_2 capture is ~10 wt % in our system.

Reaction mechanisms and chemical equilibria for CO_2 capture in PEI and NOHM-I-PEI

Quantitative ^{13}C NMR (Fig. 2A) quantitively assessed the carbon species after CO_2 capture in PEI and NOHM-I-PEI solutions. Figure 2B summarizes our proposed mechanism for CO_2 capture by the NOHM-I-PEI composites as discerned from ^{1}H NMR results (middle of Fig. 2B) and ^{13}C NMR results (right-hand side of Fig. 2B). The structure of NOHM-I-PEI dissolved in D_2O (10 wt %) was studied by ^{13}C NMR with fully assigned peaks spanning the range of 36 to 56 parts per million (ppm), as shown in Fig. 1B. Likewise, the structure of PEI (8 wt % in D_2O) was also studied with the fully assigned ^{13}C spectrum shown in fig. S5, which is consistent with the results reported previously (*41*). The nearly identical spectra for NOHM-I-PEI and pure PEI indicate that the presence of silica has negligible effects on the chemical environment of PEI.

Carbon-13 NMR provides the most direct assessment of the mechanisms shown in Fig. 2B. Resonance peaks in the range of 36.4 to 55.8 ppm are omitted from display because they are easily assigned to polymer carbons with characteristic chemical shifts of PEI backbone carbons (Fig. 1B and fig. S5). Free CO_2 species are characterized by a chemical shift of 124.5 ppm (*42*). The 0.8 wt % PEI-D_2O-$^{13}CO_2$ sample exhibits a weak peak at ~124.5 ppm consistent with dissolved $^{13}CO_2$, and there is also an intense and narrow peak at 160.3 ppm (figs. S6 and S7) that is assigned to HCO_3^-/CO_3^{2-} species (*43*). Because of the rapid equilibration between the bicarbonate and carbonate ions (Eq. 5), the peaks for these two ions appear as a single peak whose frequency offset depends on the relative amounts between

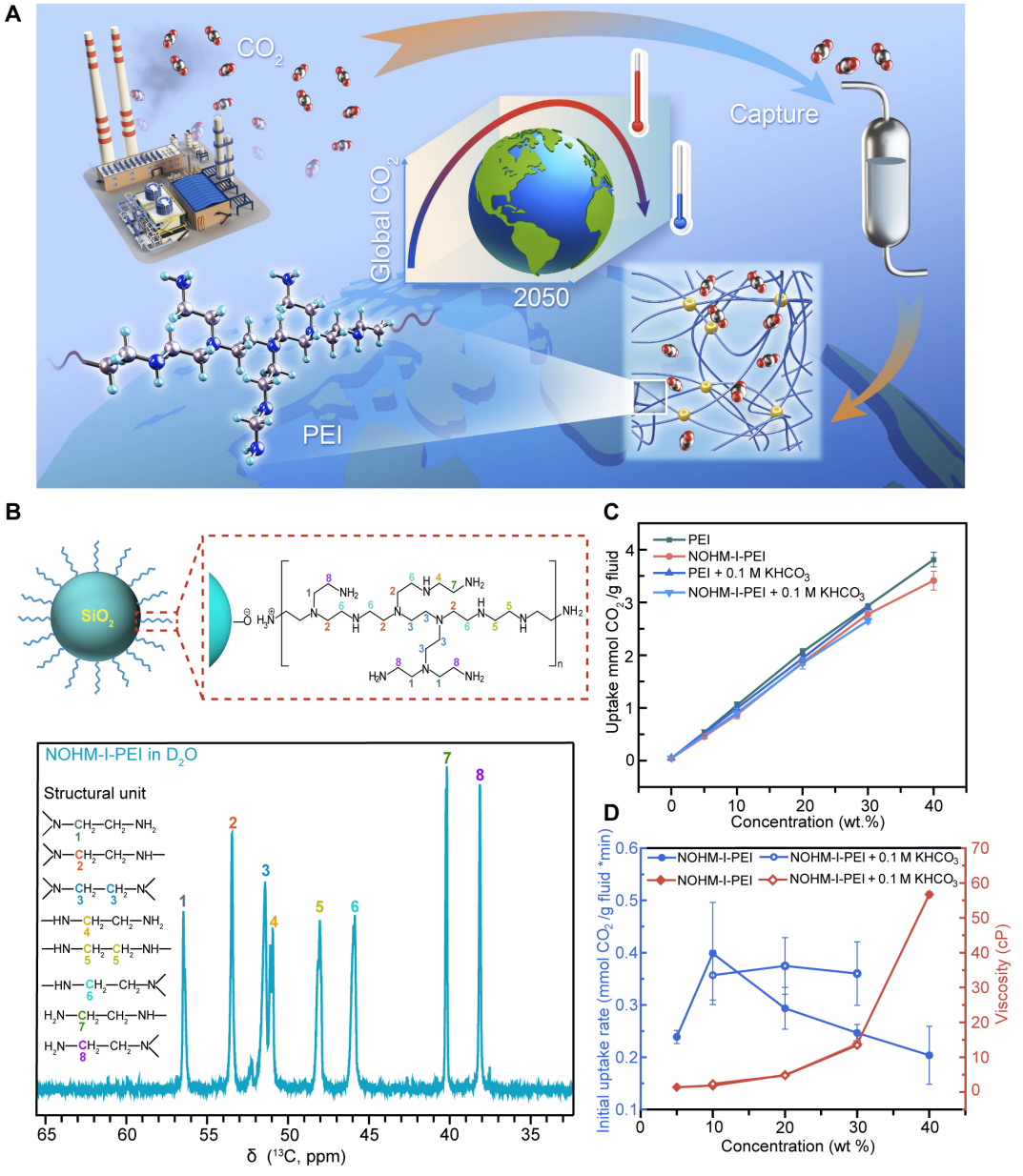

Fig. 1. CO_2 capture in branched polyethylenimine modified nano-silica (NOHM-I-PEI). (**A**) Schematic of CO_2 capture in NOHM-I-PEI solution. (**B**) Chemical structure and one-dimensional (1D) ^{13}C nuclear magnetic resonance (NMR) spectrum of NOHM-I-PEI in D_2O [structural units: inset in (B)] measured at room temperature (~22°C). (**C**) CO_2 capture capacity and (**D**) initial CO_2 capture rate and viscosity of PEI-based and NOHM-I-PEI–based fluids/electrolytes as a function of polymer concentration.

them [equation 9 shown in (*44*) was supposed to be $[HCO_3^-]/[CO_3^{2-}] = (S - 168.09)/(160.33 - S)$ with S being the chemical shift of HCO_3^-/CO_3^{2-}]. Thus, the molar ratio of CO_3^{2-} to HCO_3^- is seen to increase with the concentration of PEI or NOHM-I-PEI solution (figs. S8 and S9), as evidenced by higher frequency shifts at a higher PEI or NOHM-I-PEI concentration (*43*, *44*). A collection of peaks also appears at ~164.7 ppm that we associate with reaction products of CO_2 with amines, i.e., carbamates (^{15}N NMR data confirm this assignment, vide infra; as detailed in figs. S10 and S11) (*45*).

Upon fitting the peaks located in the range of 163 to 165 ppm for PEI after $^{13}CO_2$ capture, two peaks at 164.4 and 163.6 ppm can be assigned to primary and secondary amine-derived carbamate (fig. S12) (*46*, *47*), respectively. Both primary (α) and secondary (β) amine-derived carbamate peaks are split into two peaks, likely due to the unreacted neighboring amino groups (moieties shown on the top in fig. S12) (*46*, *47*). To further prove the assignment of the α- and β-carbamate species, linear PEI (LPEI), mainly consisting of secondary amines with a small number of primary amines, is compared with branched PEI after CO_2 absorption (fig. S13). The carbamate resonance in LPEI after $^{13}CO_2$ absorption, mainly appearing around 163.6 ppm, is assigned to β-carbamates, while the higher-frequency, weaker peak at 164.4 ppm belongs to the α-carbamates

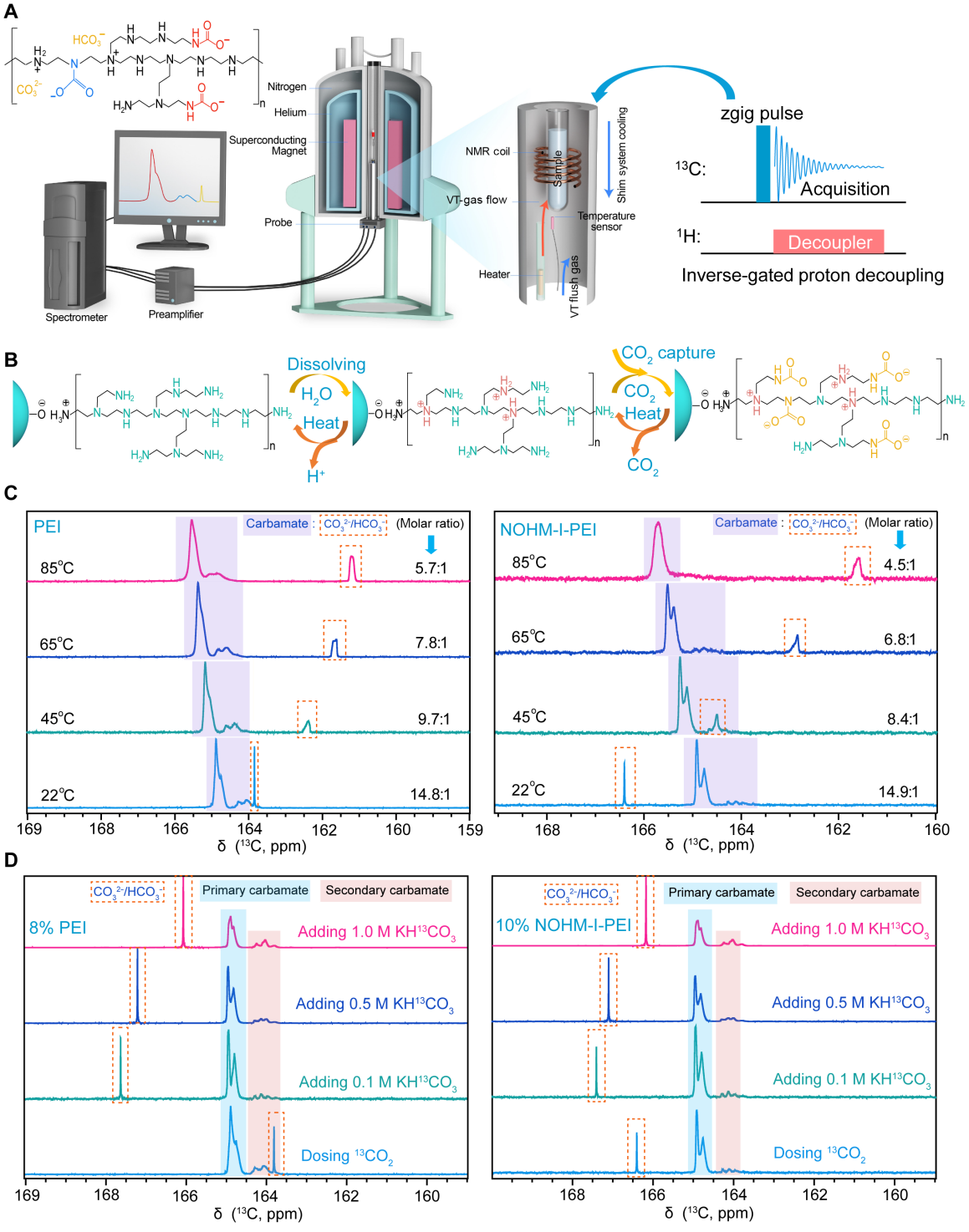

Fig. 2. ^{13}C NMR measurements of PEI and NOHM-I-PEI solutions at variable temperatures. (**A**) Schematic of ^{13}C NMR measurements in polymer solutions at variable temperatures (VT). (**B**) Chemical reactions on polymer before and after CO_2 capture. (**C**) Quantification of carbon species in 8 wt % PEI-D_2O and 10 wt % NOHM-I-PEI–D_2O solutions after $^{13}CO_2$ capture via ^{13}C NMR at variable temperatures. (**D**) 1D ^{13}C NMR spectra of 8 wt % PEI and 10 wt % NOHM-I-PEI in D_2O loaded with $^{13}CO_2$ or different concentrations of $KH^{13}CO_3$ at room temperature (~22°C).

(located at the end of the LPEI chain). Although dissolved in different solvents (LPEI is not soluble in D_2O at room temperature), the carbamate resonances appear to have the same chemical shifts in both deuterium-substituted methanol (MeOD-d4) and water (D_2O). Dissolved CO_2 can also react with MeOD to form $MeOCO_2^-$ in nonaqueous solvents (*48*), as is apparent in fig. S13. In addition, because of the protonation of amino groups in PEI, the 8 wt % PEI solution presents a high pH value (~11.4; figs. S14 and S15) that facilitates the reaction between HCO_3^- and OH^- to form CO_3^{2-} (Eq. 5).

The present results are informed by considering the equilibrium reactions involved in the absorption of $^{13}CO_2$ in both PEI and NOMH-I-PEI solution, as follows (*49*–*51*).

Protonation reactions before CO_2 absorption

$$RNH_2 + H_2O \rightleftharpoons OH^- + RNH_3^+ \quad (1)$$

$$RR'NH + H_2O \rightleftharpoons OH^- + RR'NH_2^+ \quad (2)$$

$$RR'R''N + H_2O \rightleftharpoons OH^- + RR'R''NH^+ \quad (3)$$

Carbamate formation reactions after CO_2 absorption

$$CO_2 + OH^- \rightleftharpoons HCO_3^- \quad (4)$$

$$HCO_3^- + OH^- \rightleftharpoons CO_3^{2-} + H_2O \quad (5)$$

$$RNH_2 + HCO_3^- \rightleftharpoons RNHCOO^- + H_2O \quad (6)$$

$$RR'NH + HCO_3^- \rightleftharpoons RR'NCOO^- + H_2O \quad (7)$$

$$CO_2 + 2RNH_2 \rightleftharpoons RNHCOO^- + RNH_3^+ \quad (8)$$

$$CO_2 + 2RR'NH \rightleftharpoons RR'NCOO^- + RRNH_2^+ \quad (9)$$

In these chemical equilibria, the R (R′ or R″) groups represent the rest of the organic polymer. As PEI contains primary, secondary, and tertiary amines, it enables several reaction pathways with CO_2 or HCO_3^- to form the products listed above [e.g., —CH_2CH_2—$NHCOO^-$, (—CH_2CH_2—)$_2NCOO^-$, and (—CH_2CH_2—)$_3NH^+$].

The high pH of the polymer solution (fig. S14) facilitates the conversion of CO_2 to HCO_3^-, CO_3^{2-}, and carbamate species in PEI or NOHM-I-PEI solution (*47*). To quantitate the ratio of carbon species after $^{13}CO_2$ absorption, the ^{13}C NMR spectrum was collected using inverse gated decoupling with adequate recycle delay (108 to 360 s) to ensure total spin-lattice (T_1) relaxation. On the basis of the integrated peak areas from the ^{13}C NMR at variable temperatures (Fig. 2C), the molar ratio between carbonate/bicarbonate (CO_3^{2-}/HCO_3^-) and carbamate (RHNCOO$^-$ or RR′NCOO$^-$) moieties increases with temperature from 22° to 85°C (Fig. 2C), suggesting a dynamic conversion between the carbamate and bicarbonate species in the polymer solution at elevated temperature (reverse reactions of Eqs. 6 and 7). In addition, the CO_3^{2-}/HCO_3^- resonance shifts to a lower frequency, indicating an increased ratio of HCO_3^- to CO_3^{2-} when increasing the temperature (reverse reaction of Eq. 5) or increasing the concentration of added $KH^{13}CO_3$ (Fig. 2D; as detailed in the fig. S9 caption). The net result of increasing temperature is to drive the equilibria for Eqs. 5 to 7 to favor bicarbonate species (reverse reactions), thereby shifting the equilibria in Eq. 4 toward CO_2. The electrochemical reactor implications are clear: The thermal regeneration of NOHM-I-PEI–CO_2 solutions is more favorably operated near 60° or 80°C with accompanying dissociation of carbamate for electrochemical applications (*24*).

Transport properties of PEI and NOHM-I-PEI solutions and the impact of CO_2 capture

Besides the reaction mechanisms and the chemical equilibria for CO_2 capture in PEI or NOHM-I-PEI solutions, the influence of CO_2 capture on bulk properties is also of great interest as they are vital factors for electrolytes that determine macroscopic operating electrochemical unit design. When studying the conductivity of PEI and NOHM-I-PEI solutions at different water contents, it is apparent that after CO_2 absorption, the conductivity of both PEI and NOHM-I-PEI solutions have been enhanced 20-fold (Fig. 3A, fig. S16A, and tables S2 and S3). The considerably enhanced conductivity is ascribed to the formation of several charged species after CO_2 chemisorption, including the carbamate anion (RNHCOO$^-$ and RR′NCOO$^-$), protonated cation (RNH_3^+ and $RR'NH_2^+$), bicarbonate ion (HCO_3^-), and carbonate ion (CO_3^{2-}) (Eqs. 4 to 9) (*52*). The presence of silica appears to have little to no effect on the conductivity in solutions of NOHM-I-PEI (Fig. 3A). At a more microscopic level, the question becomes what role charges on the PEI chains play in conductivity. By using electrophoretic NMR, we observed that, when adding $KHCO_3$ to PEI and NOHM-I-PEI solutions, the electrophoretic mobility of PEI increased (fig. S17), further demonstrating that the polymer chains acquired negatively charged carbamates after amines react with HCO_3^-. With the addition of the potassium salt, K^+ may tailor the electrochemical double layer by pairing with RNHCOO$^-$ or RR′NCOO$^-$ and facilitate the electron transfer from the cathode through K^+ to RNHCOO$^-$ or RR′NCOO$^-$, influencing the conversion of carbamates into higher-value carbon molecules according to the literature (*24*).

The mass transport properties of PEI and NOHM-I-PEI solutions are studied from both macroscale and microscale aspects: viscosity and self-diffusion. The bulk viscosity measurements of both PEI and NOHM-I-PEI solutions are consistent with the hypothesis that PEI chains entangle at a higher concentration (i.e., lower water content) and present increased hydrodynamic radii when tethered to silica particles. For example, the viscosity of both PEI and NOHM-I-PEI solutions increases as the water content decreases (Fig. 3B), consistent with increasing PEI chain entanglement. Either before or after CO_2 absorption, at the same water content, NOHM-I-PEI solution shows a higher viscosity than that of PEI solution (Fig. 3B). In addition, NOHM-I-PEI has an enhanced viscosity gap (the viscosity difference of the same sample before and after CO_2 absorption at the same concentration or water content; Fig. 3B and fig. S16B) compared with PEI solution. The above results demonstrate that the addition of silica particles to PEI leads to a higher viscosity, attributed to the increased hydrodynamic radii of the grafted nanoparticle units compared to untethered polymer solutions and restrictions on polymer mobility imposed by space-filling requirements (see molecular dynamics simulations below). This is consistent with our previous studies on NOHMs viscosity (*53*, *54*).

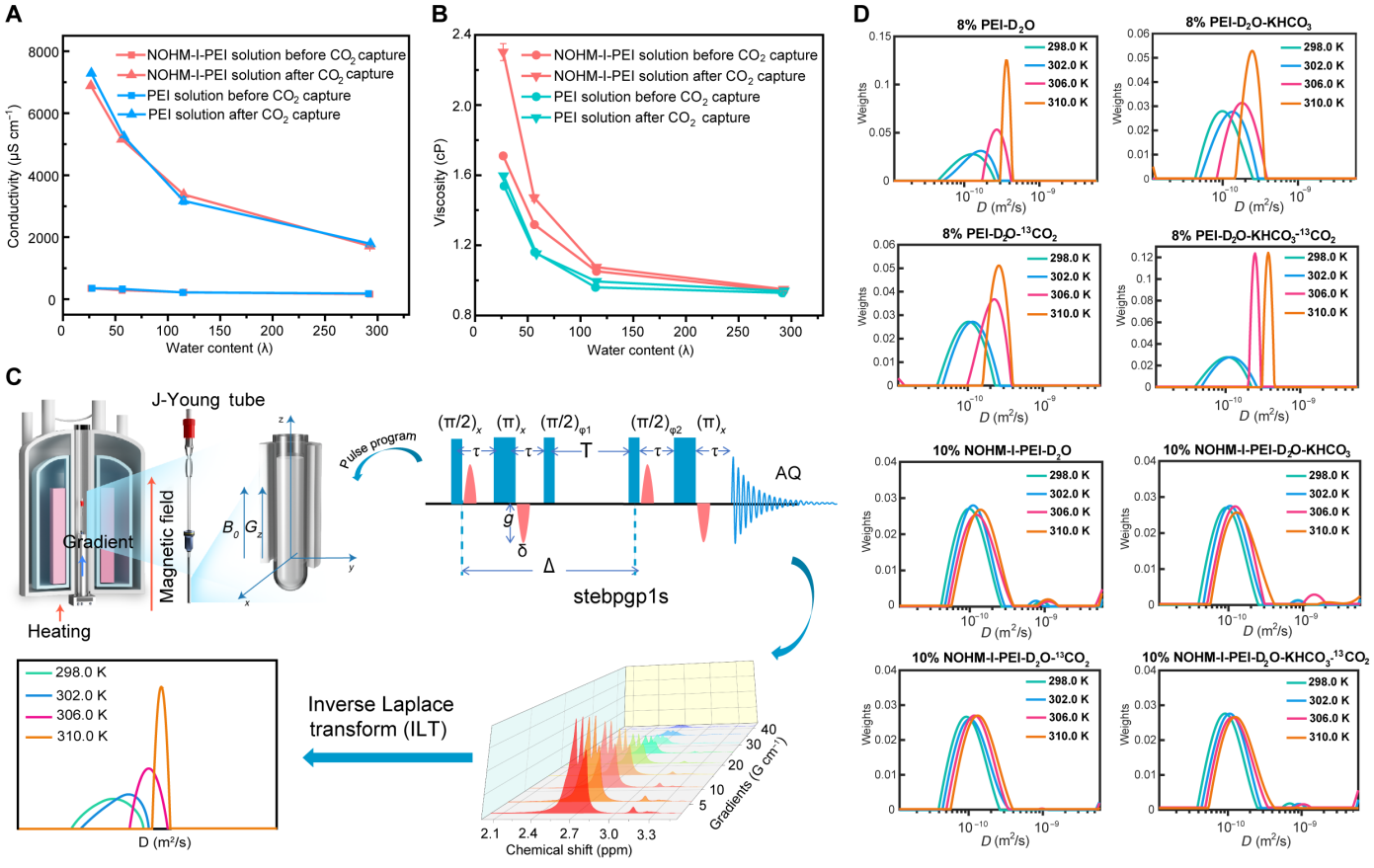

Fig. 3. Transport properties of PEI-based and NOHM-I-PEI–based electrolyte solutions. (**A**) Conductivity and (**B**) viscosity of PEI and NOHM-I-PEI solutions before and after CO_2 capture. (**C**) Schematic of ^{1}H pulsed-field-gradient (PFG) NMR measurements in polymer solutions at variable temperatures. (**D**) Distribution of self-diffusion coefficient of 8 wt % PEI and 10 wt % NOHM-I-PEI solutions before and after CO_2 capture with or without the addition of $KHCO_3$ at variable temperatures.

Last, the viscosity of the aqueous PEI solutions remained relatively unchanged before and after CO_2 capture (Fig. 3B); conversely, the viscosity in NOHM-I-PEI solutions after CO_2 capture is much higher than that of the NOHM-I-PEI solution before CO_2 absorption (which was especially noticeable at a concentration higher than 5 wt % (fig. S16B) or water content below 115 (Fig. 3B). Thus, these findings revealed that carbamate formation from CO_2 chemisorption reactions affects transport properties of NOHM-based electrolyte solutions, a notable concern in electrochemical device design.

At the microscale, we measured the self-diffusion coefficients of polymer via pulsed-field-gradient (PFG) NMR based on the ethylene protons in the PEI units (blue integrated area in fig. S18) or NOHM-I-PEI (blue integrated area in fig. S19). The distribution of self-diffusion coefficients in our polymer solutions is analyzed by Laplace inversion (ILT) (*55*) of the Stejskal-Tanner plots (Fig. 3C) (*56*). The mean self-diffusion coefficients (peak value of self-diffusion coefficients in Fig. 3D) for both PEI and NOHM-I-PEI solutions increase slightly with temperature and follow an Arrhenius-like behavior over the investigated temperature range (298.0 to 310.0 K) (fig. S20, A to C). The activation energy of self-diffusion for PEI solution is calculated to be 17.6 kJ mol^{-1}, reaching 37.4 kJ mol^{-1} when $KHCO_3$ and CO_2 were introduced. Here, we surmise that the formation of negatively charged carbamates and positively charged ammonium on the polymer chains (Eqs. 8 and 9) leads to coulombic interactions between carbamate and ammonium in different polymer chains, thereby hindering the self-diffusion of polymer chains and presenting higher activation energies. In contrast, the activation energies for the four NOHM-I-PEI samples (NOHM-I-PEI solution before and after CO_2 capture with or without the addition of $KHCO_3$) are almost the same (fig. S20C): Self-diffusion of PEI depends on the silica nanoparticles whereon the PEI is tethered.

An advantage of the ILT method is the determination of the distribution width of derived parameters; in the present case is the self-diffusion coefficients (Fig. 3D). While polydispersity may play some role (fig. S21), we cannot account for the observed distributions of D_{self} without considering other factors (*57*). The width of the distribution of the self-diffusion coefficients of the PEI solution decreases monotonically with temperature (fig. S20B); in contrast, the width of the distribution of the self-diffusion coefficients of NOHM-I-PEI stays the same (fig. S20D). This is expected as the transport properties of bound PEI are expected to be dominated by silica particles due to the smaller size of PEI (~2 nm) compared with that of silica (~10 nm). Similar trends of temperature-dependent self-diffusion coefficients and their distribution width are also observed in lower concentrations of PEI solution (fig. S22) or PEI solution treated with HCl (figs. S23 and S24). These findings demonstrate that the self-diffusion properties of NOHM-I-PEI are dominated by silica nanoparticles rather than PEI.

We quantitatively elucidate the correlation between the dynamics and the state of PEI chains by molecular dynamics simulation of the protonation and carbamation on PEI chains. The size of PEI increases monotonically with the chain protonation fraction due to the more pronounced intra-chain repulsion (Fig. 4, A to C). Consequently, the self-diffusion coefficients decrease with chain protonation fraction (Fig. 4D), in qualitative agreement with experimental results. This occurs in both moderately (fig. S25) and highly branched (fig. S26) chains used here, as well as linear chains reported in the literature (*58*, *59*). Therefore, the dependence of chain size and self-diffusion coefficient on protonation fraction is qualitatively not affected by the degree of branching of PEI, an important factor in industrial scale sourcing of PEI. After adding potassium bicarbonate or introducing CO_2, negatively charged carbamates form on PEI or NOHM-I-PEI, with the resulting accumulation of negative carbamates on PEI chains yielding higher charge repulsion and increasing the polymer size (Fig. 4, E to G). However, unlike chain protonation, further carbamation does not monotonically increase the chain size. At a very high chain carbamate fraction (0.75), the PEI chain does not extend but contracts as a single counterion (Na^+, K^+) tends to bind multiple carbamate groups (fig. S27). The self-diffusion coefficients accordingly decrease rapidly when increasing the chain carbamate fraction at first but remain stable or increase slightly when the fraction is over 0.2 (Fig. 4H). We surmise that this non-monotonic relationship explains the results in Fig. 3D where the mean diffusion coefficient of PEI is larger than that of PEI with the addition of CO_2 or $KHCO_3$ (lower fraction of carbamate) yet slightly lower than that of PEI with the addition of both CO_2 and $KHCO_3$ (higher fraction of carbamate) at 310.0 K. PEI chains in NOHM-I-PEI probably share the same properties due to the same mechanism of forming carbamate. Therefore, both protonation and carbamation have an essential influence on the self-diffusion coefficient of PEI chains, implying a nontrivial interplay between the dynamics of PEI and electrolyte speciation.

In summary, we provide direct evidence that the temperature determines the ratio of CO_2-chemisorbed products in both PEI and NOHM-I-PEI solutions by variable temperature quantitative ^{13}C NMR. The molar ratio between carbonate/bicarbonate (CO_3^{2-}/HCO_3^-) and carbamates ($RHNCOO^-$ and $RR'NCOO^-$) (i.e., chemisorbed carbon species) increased with the temperatures (22° to 85°C) and the CO_3^{2-}/HCO_3^- equilibrium ^{13}C NMR peak shifted to a lower frequency, indicating reversible conversion between carbamates and carbonate/bicarbonate, thereby suggesting the more favorable operation near 60° or 80°C for potential integrated electrochemical applications. Combining ^1H PFG NMR techniques and inverse Laplace analysis, the average and distribution of self-diffusion coefficients of

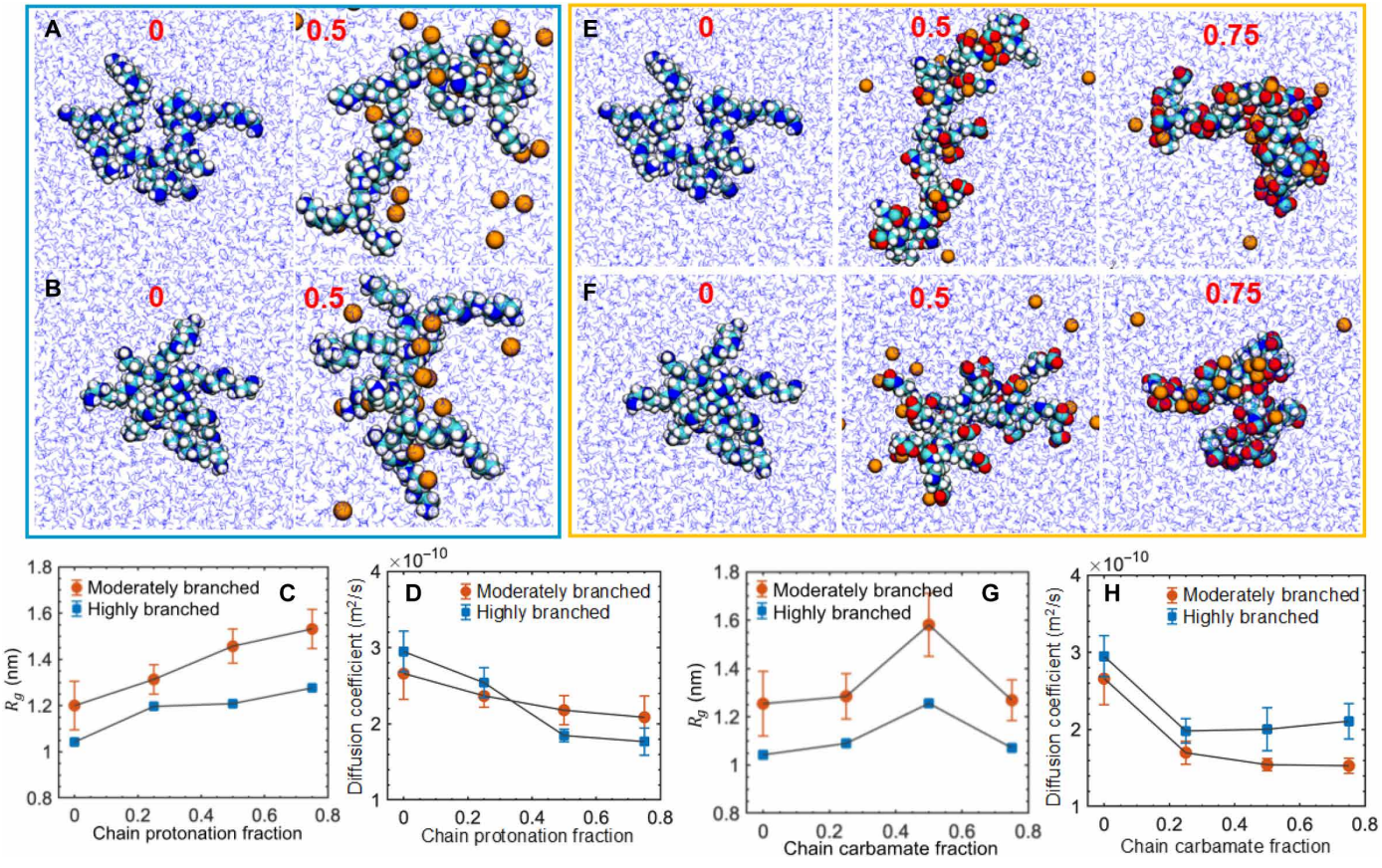

Fig. 4. Molecular dynamics of protonation and carbamation on radius of gyration (R_g) and self-diffusion coefficients. (**A**) Moderately and (**B**) highly branched PEI with protonation fractions of 0 and 0.5. (**C**) The size and (**D**) self-diffusion coefficient of PEI as a function of chain protonation fraction in moderately and highly branched PEI. (**E**) Moderately and (**F**) highly branched PEI with chain carbamate fractions of 0, 0.5, and 0.75. (**G**) The size and (**H**) self-diffusion coefficient of PEI as a function of chain carbamate fraction in moderately and highly branched PEI.

PEI and NOHM-I-PEI at different conditions (temperature, $^{13}CO_2$ absorption, the addition of $KHCO_3$, and polymer concentrations) have been obtained and activation energies discerned. The self-diffusion in the PEI systems is determined by the PEI chain states where the columbic interactions formed between the chains of negatively charged carbamates and those of positively charged ammonium, while, in the NOHM-I-PEI systems, the self-diffusion merely depends on the silica nanoparticles whereon the PEI chains are tethered. Protonation of PEI chains leads to a lower mean self-diffusion coefficient that is further proved by molecular dynamics calculations. This work has revealed the mechanism of CO_2 absorption in PEI and NOHM-I-PEI solutions by distinguishing and quantifying the species generated after CO_2 capture, as well as probing the role of PEI and NOHM-I-PEI self-diffusion mechanisms on mass transfer limitation. These insights are expected to assist in the design of efficient electrolytes combining CO_2 chemisorption and electroconversion.

MATERIALS AND METHODS

NOHM-I-PEI was synthesized by tethering PEI onto the surface of silica nanoparticles, as previously reported (*27*, *29*). The CO_2 capture capacity of various PEI and NOHM-I-PEI solutions with co-adding electrolytes was measured on the homemade setup (fig. S1). The pH, viscosities, and conductivity of PEI-based and NOHM-I-PEI–based solutions were measured by using a pH meter, a piston-based viscometer, and a conductivity meter, respectively. PEI and NOHM-I-PEI samples for NMR measurements were prepared by dissolving them in D_2O. Variable temperature quantitative ^{13}C NMR spectra were recorded on Bruker Avance I 500-MHz NMR spectrometer equipped with a 5-mm ^{1}H/BB Smart solution probe (Broadband Observe), while ^{1}H PFG and electrophoretic NMR experiments were performed on Bruker Avance I 700-MHz NMR spectrometer equipped with a 5-mm triple resonance $^{1}H/^{13}C/^{15}N$ TXI solution probe. The ^{1}H-^{15}N heteronuclear multi-bond correlation (HMBC) spectra were collected on a Bruker Avance II 900-MHz NMR spectrometer equipped with a proton-optimized triple resonance NMR inverse cryoprobe (CP TCI) with the temperature set to 298 K. Additional explanatory text including an extended technical description of results can be found in the Supplementary Materials.

Supplementary Materials

This PDF file includes:

Supplementary Text
Figs. S1 to S27
Tables S1 to S3
References

REFERENCES AND NOTES

1. G. T. Rochelle, Amine scrubbing for CO_2 capture. *Science* **325**, 1652–1654 (2009).
2. D. J. Heldebrant, P. K. Koech, V. A. Glezakou, R. Rousseau, D. Malhotra, D. C. Cantu, Water-lean solvents for post-combustion CO2 Capture: Fundamentals, uncertainties, opportunities, and outlook. *Chem. Rev.* **117**, 9594–9624 (2017).
3. M. E. Boot-Handford, J. C. Abanades, E. J. Anthony, M. J. Blunt, S. Brandani, N. Mac Dowell, J. R. Fernández, M. C. Ferrari, R. Gross, J. P. Hallett, R. S. Haszeldine, P. Heptonstall, A. Lyngfelt, Z. Makuch, E. Mangano, R. T. J. Porter, M. Pourkashanian, G. T. Rochelle, N. Shah, J. G. Yao, P. S. Fennell, Carbon capture and storage update. *Energ. Environ. Sci.* **7**, 130–189 (2014).
4. D. J. Heldebrant, J. Kothandaraman, N. Mac Dowell, L. Brickett, Next steps for solvent-based CO_2 capture; integration of capture, conversion, and mineralisation. *Chem. Sci.* **13**, 6445–6456 (2022).
5. S. R. Sinsel, R. L. Riemke, V. H. Hoffmann, Challenges and solution technologies for the integration of variable renewable energy sources—A review. *Renew. Energy* **145**, 2271–2285 (2020).
6. G. Glenk, S. Reichelstein, Economics of converting renewable power to hydrogen. *Nat. Energy* **4**, 216–222 (2019).
7. I. Sullivan, A. Goryachev, I. A. Digdaya, X. Li, H. A. Atwater, D. A. Vermaas, C. Xiang, Coupling electrochemical CO_2 conversion with CO_2 capture. *Nat. Catal.* **4**, 952–958 (2021).
8. Y. Y. Birdja, E. Pérez-gallent, M. C. Figueiredo, A. J. Göttle, F. Calle-vallejo, M. T. M. Koper, Advances and challenges in understanding the electrocatalytic conversion of carbon dioxide to fuels. *Nat. Energy* **4**, 732–745 (2019).
9. M. B. Ross, P. De Luna, Y. Li, C. Dinh, D. Kim, P. Yang, E. H. Sargent, Designing materials for electrochemical carbon dioxide recycling. *Nat. Catalysis* **2**, 648–658 (2019).
10. Y. Wu, Z. Jiang, X. Lu, Y. Liang, H. Wang, Domino electroreduction of CO_2 to methanol on a molecular catalyst. *Nature* **575**, 639–642 (2019).
11. M. Ko, J. Vaes, E. Klemm, D. Pant, Solvents and supporting electrolytes in the electrocatalytic reduction of CO_2. *iScience* **19**, 135–160 (2019).
12. L. Fan, C. Xia, F. Yang, J. Wang, H. Wang, Y. Lu, Strategies in catalysts and electrolyzer design for electrochemical CO_2 reduction toward C_{2+} products. *Sci. Adv.* **6**, eaay3111 (2020).
13. D. H. Nam, P. De Luna, A. Rosas-Hernández, A. Thevenon, F. Li, T. Agapie, J. C. Peters, O. Shekhah, M. Eddaoudi, E. H. Sargent, Molecular enhancement of heterogeneous CO_2 reduction. *Nat. Mater.* **19**, 266–276 (2020).
14. A. Wagner, C. D. Sahm, E. Reisner, Towards molecular understanding of local chemical environment effects in electro- and photocatalytic CO_2 reduction. *Nat. Catalysis* **3**, 775–786 (2020).
15. D. Wakerley, S. Lamaison, J. Wicks, A. Clemens, J. Feaster, D. Corral, S. A. Jaffer, A. Sarkar, M. Fontecave, E. B. Duoss, S. Baker, E. H. Sargent, T. F. Jaramillo, C. Hahn, Gas diffusion electrodes, reactor designs and key metrics of low-temperature CO_2 electrolysers. *Nat. Energy* **7**, 130–143 (2022).
16. E. W. Lees, B. A. W. Mowbray, F. G. L. Parlane, C. P. Berlinguette, Gas diffusion electrodes and membranes for CO_2 reduction electrolysers. *Nat. Rev. Mater.* **7**, 55–64 (2022).
17. C. V. Amanchukwu, The electrolyte frontier: A manifesto. *Joule* **4**, 281–285 (2020).
18. B. A. Rosen, J. L. Haan, P. Mukherjee, B. Braunschweig, W. Zhu, A. Salehi-Khojin, D. D. Dlott, R. I. Masel, In situ spectroscopic examination of a low overpotential pathway for carbon dioxide conversion to carbon monoxide. *J. Phys. Chem. C* **116**, 15307–15312 (2012).
19. B. A. Rosen, I. Hod, Tunable molecular-scale materials for catalyzing the low-overpotential electrochemical conversion of CO_2. *Adv. Mater.* **30**, e1706238 (2018).
20. B. A. Rosen, A. Salehi-Khojin, M. R. Thorson, W. Zhu, D. T. Whipple, P. J. A. Kenis, R. I. Masel, Ionic liquid-mediated selective conversion of CO2 to CO at low overpotentials. *Science* **334**, 643–644 (2011).
21. Z. P. Jovanov, J. F. De Araujo, S. Li, P. Strasser, Catalyst preoxidation and EDTA electrolyte additive remedy activity and selectivity declines during electrochemical CO_2 reduction. *J. Phys. Chem. C* **123**, 2165–2174 (2019).
22. D. V. Vasilyev, A. V. Rudnev, P. Broekmann, P. J. Dyson, A general and facile approach for the electrochemical reduction of carbon dioxide inspired by deep eutectic solvents. *ChemSusChem* **12**, 1635–1639 (2019).
23. M. Abdinejad, Z. Mirza, X. Zhang, H. Kraatz, Enhanced electrocatalytic activity of primary amines for CO_2 reduction using copper electrodes in aqueous solution. *ACS Sustain. Chem. Eng.* **8**, 1715–1720 (2020).
24. G. Lee, Y. C. Li, J. Y. Kim, T. Peng, D. H. Nam, A. Sedighian Rasouli, F. Li, M. Luo, A. H. Ip, Y. C. Joo, E. H. Sargent, Electrochemical upgrade of CO_2 from amine capture solution. *Nat. Energy* **6**, 46–53 (2021).
25. E. Pérez-Gallent, C. Vankani, C. Sánchez-Martínez, A. Anastasopol, E. Goetheer, Integrating CO_2 capture with electrochemical conversion using amine-based capture solvents as electrolytes. *Ind. Eng. Chem. Res.* **60**, 4269–4278 (2021).
26. S. Srivastava, S. Choudhury, A. Agrawal, L. A. Archer, Self-suspended polymer grafted nanoparticles. *Curr. Opin. Chem. Eng.* **16**, 92–101 (2017).
27. K.-Y. A. Lin, A.-H. A. Park, Effects of bonding types and functional groups on CO_2 capture using novel multiphase systems of liquid-like nanoparticle organic hybrid materials. *Environ. Sci. Technol.* **45**, 6633–6639 (2011).
28. Y. Park, K.-Y. A. Lin, A.-H. A. Park, C. Petit, Recent advances in anhydrous solvents for CO_2 capture: Ionic liquids, switchable solvents, and nanoparticle organic hybrid materials. *Front. Energy Res.* **3**, 1–14 (2015).
29. G. Rim, T. G. Feric, T. Moore, A. H. A. Park, Solvent impregnated polymers loaded with liquid-like nanoparticle organic hybrid materials for enhanced kinetics of direct air capture and point source CO_2 capture. *Adv. Funct. Mater.* **31**, 2010047 (2021).
30. S. Overa, T. G. Feric, A. H. A. Park, F. Jiao, Tandem and hybrid processes for carbon dioxide utilization. *Joule* **5**, 8–13 (2021).
31. T. G. Feric, S. T. Hamilton, A.-H. A. Park, Insights into the enhanced oxidative thermal stability of nanoparticle organic hybrid materials developed for carbon capture and energy storage. *Energy Fuels* **35**, 19592–19605 (2021).

32. T. G. Feric, S. T. Hamilton, B. H. Ko, G. A. Lee, S. Verma, F. Jiao, A. H. A. Park, Highly tunable syngas product ratios enabled by novel nanoscale hybrid electrolytes designed for combined CO_2 capture and electrochemical conversion. *Adv. Funct. Mater.* **33**, 2210017 (2023).
33. Y. Park, J. Decatur, K.-Y. A. Lin, A.-H. A. Park, Investigation of CO_2 capture mechanisms of liquid-like nanoparticle organic hybrid materials via structural characterization. *Phys. Chem. Chem. Phys.* **13**, 18115–18122 (2011).
34. C. Petit, Y. Park, K.-Y. A. Lin, A.-H. A. Park, Spectroscopic investigation of the canopy configurations in nanoparticle organic hybrid materials of various grafting densities during CO_2 capture. *J. Phys. Chem. C* **116**, 516–525 (2012).
35. M. D. Tikekar, S. Choudhury, Z. Tu, L. A. Archer, Design principles for electrolytes and interfaces for stable lithium-metal batteries. *Nat. Energy* **1**, 16114 (2016).
36. S. Choudhury, A. Agrawal, S. Wei, E. Jeng, L. A. Archer, Hybrid hairy nanoparticle electrolytes stabilizing lithium metal batteries. *Chem. Mater.* **28**, 2147–2157 (2016).
37. Y. Bai, M. S. Schaberg, S. J. Hamrock, Z. Tang, G. Goenaga, A. B. Papandrew, T. A. Zawodzinski, Density measurements and partial molar volume analysis of different membranes for polymer electrolyte membrane fuel cells. *Electrochim. Acta* **242**, 307–314 (2017).
38. B. Lv, B. Guo, Z. Zhou, G. Jing, Mechanisms of CO_2 capture into monoethanolamine solution with different CO_2 loading during the absorption/desorption processes. *Environ. Sci. Technol.* **49**, 10728–10735 (2015).
39. P. V. Kortunov, M. Siskin, L. S. Baugh, D. C. Calabro, *In situ* nuclear magnetic resonance mechanistic studies of carbon dioxide reactions with liquid amines in aqueous systems: New insights on carbon capture reaction pathways. *Energy Fuel* **29**, 5919–5939 (2015).
40. P. V. Kortunov, M. Siskin, M. Paccagnini, H. Thomann, CO_2 reaction mechanisms with hindered alkanolamines: Control and promotion of reaction pathways. *Energy Fuel* **30**, 1223–1236 (2016).
41. T. S. Pierre, M. Geckle, 13-NMR analysis of branched polyethyleneimine. *J. Macromol. Sci. Chem.* **22**, 877–887 (1985).
42. M. L. Pinto, L. Mafra, J. M. Guil, J. Pires, J. Rocha, Adsorption and activation of CO_2 by amine-modified nanoporous materials studied by solid-state NMR and $^{13}CO_2$ adsorption. *Chem. Mater.* **23**, 1387–1395 (2011).
43. F. Mani, M. Peruzzini, P. Stoppioni, CO_2 absorption by aqueous NH_3 solutions: Speciation of ammonium carbamate, bicarbonate and carbonate by a ^{13}C NMR study. *Green Chem.* **8**, 995–1000 (2006).
44. P. E. Holmes II, M. Naaz, B. E. Poling, Ion concentrations in the CO_2-NH_3-H_2O system from ^{13}C NMR spectroscopy. *Ind. Eng. Chem. Res.* **37**, 3281–3287 (1998).
45. A. F. Ciftja, A. Hartono, H. F. Svendsen, Experimental study on carbamate formation in the AMP-CO_2-H_2O system at different temperatures. *Chem. Eng. Sci.* **107**, 317–327 (2014).
46. C. Perinu, I. M. Bernhardsen, D. D. D. Pinto, H. K. Knuutila, K. Jens, NMR speciation of aqueous MAPA, tertiary amines, and their blends in the presence of CO_2: Influence of pK_a and reaction mechanisms. *Ind. Eng. Chem. Res.* **57**, 1337–1349 (2018).
47. R. Zhang, X. Luo, Q. Yang, H. Yu, G. Puxty, Z. Liang, Analysis for the speciation in CO_2 loaded aqueous MEDA and MAPA solution using ^{13}C NMR technology. *Int. J. Greenh. Gas Control.* **71**, 1–8 (2018).
48. P. V. Kortunov, L. S. Baugh, M. Siskin, D. C. Calabro, *In situ* nuclear magnetic resonance mechanistic studies of carbon dioxide reactions with liquid amines in mixed base systems: The interplay of lewis and Brønsted basicities. *Energy Fuel* **29**, 5967–5989 (2015).
49. F. Barzagli, F. Mani, M. Peruzzini, A ^{13}C NMR study of the carbon dioxide absorption and desorption equilibria by aqueous 2-aminoethanol and N-methyl-substituted 2-aminoethanol. *Energ. Environ. Sci.* **2**, 322–330 (2009).
50. W. Conway, X. Wang, D. Fernandes, R. Burns, G. Lawrance, G. Puxty, M. Maeder, Comprehensive kinetic and thermodynamic study of the reactions of CO_2(aq) and HCO_3^- with monoethanolamine (MEA) in aqueous solution. *J. Phys. Chem. A* **115**, 14340–14349 (2011).
51. Z. Zhang, A. L. Kummeth, J. Y. Yang, A. N. Alexandrova, Inverse molecular design of alkoxides and phenoxides for aqueous direct air capture of CO_2. *Proc. Natl. Acad. Sci. U.S.A.* **119**, e2123496119 (2022).
52. L. Chen, F. Li, Y. Zhang, C. L. Bentley, M. Horne, A. M. Bond, J. Zhang, Electrochemical reduction of carbon dioxide in a monoethanolamine capture medium. *ChemSusChem* **10**, 4109–4118 (2017).
53. T. G. Feric, S. T. Hamilton, M. A. Haque, J. Jeddi, J. Sangoro, M. D. Dadmun, A. H. A. Park, Impacts of bond type and grafting density on the thermal, structural, and transport behaviors of nanoparticle organic hybrid materials-based electrolytes. *Adv. Funct. Mater.* **32**, 2203947 (2022).
54. S. T. Hamilton, T. G. Feric, S. Bhattacharyya, N. M. Cantillo, S. G. Greenbaum, T. A. Zawodzinski, A.-H. A. Park, Nanoscale hybrid electrolytes with viscosity controlled using ionic stimulus for electrochemical energy conversion and storage. *JACS Au* **2**, 590–600 (2022).
55. L. Venkataramanan, Y. Q. Song, M. D. Hürlimann, Solving Fredholm integrals of the first kind with tensor product structure in 2 and 2.5 dimensions. *IEEE Trans. Signal Process.* **50**, 1017–1026 (2002).
56. U. Böhme, U. Scheler, Hydrodynamic size and charge of polyelectrolyte complexes. *J. Phys. Chem. B* **111**, 8348–8350 (2007).
57. E. U. Mapesa, N. M. Cantillo, S. T. Hamilton, M. A. Harris, T. A. Zawodzinski, A. H. Alissa Park, J. Sangoro, Localized and collective dynamics in liquid-like polyethylenimine-based nanoparticle organic hybrid materials. *Macromolecules* **54**, 2296–2305 (2021).
58. K. P. Sharma, C. K. Choudhury, S. Srivastava, H. Davis, P. R. Rajamohanan, S. Roy, G. Kumaraswamy, Assembly of polyethyleneimine in the hexagonal mesophase of nonionic surfactant: Effect of pH and temperature. *J. Phys. Chem. B* **115**, 9059–9069 (2011).
59. T. A. Beu, A. Farcaş, CHARMM force field and molecular dynamics simulations of protonated polyethylenimine. *J. Comput. Chem.* **38**, 2335–2348 (2017).
60. D. M. Halat, C. Fang, D. Hickson, A. Mistry, J. A. Reimer, N. P. Balsara, R. Wang, Electric-field-induced spatially dynamic heterogeneity of solvent motion and cation transference in electrolytes. *Phys. Rev. Lett.* **128**, 198002 (2022).
61. Y. Q. Song, L. Venkataramanan, M. D. Hürlimann, M. Flaum, P. Frulla, C. Straley, T_1-T_2 correlation spectra obtained using a fast two-dimensional Laplace inversion. *J. Magn. Reson.* **154**, 261–268 (2002).
62. J. Suh, B. K. Hwang, Ionization of poly(ethylenimine) and poly(allylamine) at various pH's. *Bioorg. Chem.* **22**, 318–327 (1994).
63. C. Sun, T. Tang, H. Uludağ, J. E. Cuervo, Molecular dynamics simulations of DNA/PEI complexes: Effect of PEI branching and protonation state. *Biophys. J.* **100**, 2754–2763 (2011).
64. S. Jo, T. Kim, V. G. Iyer, W. Im, CHARMM-GUI: A web-based graphical user interface for CHARMM. *J. Comput. Chem.* **29**, 1859–1865 (2008).
65. J. Huang, A. D. Mackerell, CHARMM36 all-atom additive protein force field: Validation based on comparison to NMR data. *J. Comput. Chem.* **34**, 2135–2145 (2013).
66. A. D. MacKerell, D. Bashford, M. Bellott, R. L. Dunbrack, J. D. Evanseck, M. J. Field, S. Fischer, J. Gao, H. Guo, S. Ha, D. Joseph-McCarthy, L. Kuchnir, K. Kuczera, F. T. K. Lau, C. Mattos, S. Michnick, T. Ngo, D. T. Nguyen, B. Prodhom, W. E. Reiher, B. Roux, M. Schlenkrich, J. C. Smith, R. Stote, J. Straub, M. Watanabe, J. Wiórkiewicz-Kuczera, D. Yin, M. Karplus, All-atom empirical potential for molecular modeling and dynamics studies of proteins. *J. Phys. Chem. B* **102**, 3586–3616 (1998).
67. M. J. Abraham, T. Murtola, R. Schulz, S. Páll, J. C. Smith, B. Hess, E. Lindah, Gromacs: High performance molecular simulations through multi-level parallelism from laptops to supercomputers. *SoftwareX* **1-2**, 19–25 (2015).
68. S. Miyamoto, P. A. Kollman, Settle: An analytical version of the SHAKE and RATTLE algorithm for rigid water models. *J. Comput. Chem.* **13**, 952–962 (1992).
69. G. Bussi, D. Donadio, M. Parrinello, Canonical sampling through velocity rescaling. *J. Chem. Phys.* **126**, 014101 (2007).
70. H. J. C. Berendsen, J. P. M. Postma, W. F. Van Gunsteren, A. Dinola, J. R. Haak, Molecular dynamics with coupling to an external bath. *J. Chem. Phys.* **81**, 3684–3690 (1984).
71. T. Darden, D. York, L. Pedersen, Particle mesh Ewald: AnN·log(N) method for Ewald sums in large systems. *J. Chem. Phys.* **98**, 10089–10092 (1993).
72. A. M. Varghese, G. N. Karanikolos, CO_2 capture adsorbents functionalized by amine–bearing polymers: A review. *Int. J. Greenh. Gas Control.* **96**, 103005 (2020).
73. X. Zhao, X. Hu, G. Hu, R. Bai, W. Dai, M. Fan, M. Luo, Enhancement of CO_2 adsorption and amine efficiency of titania modified by moderate loading of diethylenetriamine. *J. Mater. Chem. A* **1**, 6208–6215 (2013).
74. D. R. Holycross, M. Chai, Comprehensive NMR studies of the structures and properties of PEI polymers. *Macromolecules* **46**, 6891–6897 (2013).
75. T. Kong, G. Guo, H. Zhang, L. Gao, Post-synthetic modification of polyvinyl alcohol with a series of N-alkyl-substituted carbamates towards thermo- and CO_2-responsive polymers. *Polym. Chem.* **8**, 5769–5779 (2017).
76. J. D. Ziebarth, Y. Wang, Understanding the protonation behavior of linear polyethylenimine in solutions through Monte Carlo simulations. *Biomacromolecules* **11**, 29–38 (2010).
77. K. Hayamizu, Temperature dependence of self-diffusion coefficients of ions and solvents in ethylene carbonate, propylene carbonate, and diethyl carbonate single solutions and ethylene carbonate + diethyl carbonate binary solutions of LiPF6Studied by NMR. *J. Chem. Eng. Data* **57**, 2012–2017 (2012).

Acknowledgments: We thank A. Lund and UC Berkeley's NMR facility in the College of Chemistry (CoC-NMR) for spectroscopic assistance. We also appreciate the help from J. G. Pelton (QB3 NMR Facility) to acquire HMBC data. We also thank N. Roy for helping with CO_2 capture experiments. **Funding:** This work was supported as part of the AccelNet Collaborative Research for Sustainable Capture and Conversion of CO_2 to Chemicals and Fuels using Renewable Electrons (SCO_2RE) funded by NSF National Science Foundation 1927325 (to J.A.R. and A.-H.A.P.). Funds for the QB3 900 MHz NMR spectrometer were provided by the NIH through grant GM68933. **Author contributions:** J.A.R. and A.-H.A.P. supervised the project. Y.W., T.G.F., and J.T. designed the study, performed the experiments, analyzed the data, and composed the manuscript. C.F. and R.W. carried out molecular dynamics simulations and analyzed simulation results. S.T.H. measured the transport properties of the electrolytes; G.R., T.D., and J.O. helped with experiments. All the authors reviewed

and commented on the manuscript. **Competing interests:** The authors declare that they have no competing interest. **Data and materials availability:** All data needed to evaluate the conclusions in the paper are present in the paper and/or the Supplementary Materials. MATLAB code files have been deposited on the Reimer group website (https://reimergroup.org/data.html).

Submitted 9 August 2023
Accepted 19 March 2024
Published 19 April 2024
10.1126/sciadv.adk2350